Quantum dots for hybrid energy harvesting: from integration to piezo-phototronics

Yuljae Cho,[a] Sangyeon Pak,[b] Geon-Hyoung An,[c] Bo Hou,*[d] and SeungNam Cha*[b]

Abstract: Energy harvesting, which converts wasted environmental energy into electricity by utilizing various physical effects, has been attracted to tremendous research interests as is one of the key technologies to realize advanced electronics in the future. In this review, we introduce recent progress in the field of hybrid energy harvesting technology. In particular, we focus on a quantum dots (QD)-based hybrid energy harvesting device. Attributed to fascinating material properties that QD possess, employment of QDs into hybrid energy harvesting has shown great potential for independent and sustainable energy supply.

First, an integration of a QD solar cell into a mechanical energy harvester is discussed to harness different types of environmental energy sources simultaneously. Second, a comprehensive explanation of a piezotronic and piezo-phototronic effect is provided, which is followed by QD-based piezo-phototronic applications. Finally, we summarize recent progress that has been made in energy harvesting technology involving a photovoltaic and piezo/triboelectric effect.

Keywords: Quantum dot, hybrid energy harvesting, solar cell, mechanical energy harvesting, piezo-phototronic

1. Introduction

Energy harvesting technology is aiming for independent and sustainable energy supply for powering smart electronics, for example, sensor network and personal health care that need a wireless communication system. Over the past decades, the field of energy harvesting has been extensively studied using unique physical phenomena, such as photovoltaic, piezoelectric and triboelectric effects. Among various energy harvesting devices, a solar cell and a mechanical energy harvester are the representative devices for energy harvesting which utilize a photovoltaic effect and piezo-/triboelectric effect, respectively.[1-9]

A solar cell is unarguably a long-standing topic of energy harvesting, dating back to the late 19th century. Taking into account the loss of solar energy due to atmospheric absorption and scattering, stochastic variations, and climate effects, the average global solar irradiance to the surface of the Earth is still approximately 200 Wm^{-2}, meaning that the solar power is one of the most desirable environmental energy sources.[10-12] In contrast to the solar power, mechanical energy sources are in a variety of different forms which are not dependent on the region, climate, time, and seasons. By taking advantages of different energy forms, various types of mechanical energy harvesters for the desired application have been demonstrated, such as wearable and implantable medical devices.[13-16]

Deploying QDs into a hybrid system containing a solar cell, piezoelectric and triboelectric are still challenging in terms of the processability as well as device performance. There are several questions to be answered; (1) how we can further improve the performance of a hybrid QD energy harvesting device to be widely used in practical applications, and (2) how we can combine four physical effects, such as quantum confinement, photovoltaic, piezoelectric and triboelectric, in order to enhance the overall performance of the harvester. In this regard, two promising hybrid technologies have been introduced; (1) an integration of various energy harvesters and (2) utilization of a piezotronic/piezo-phototronic effect. These fields are experiencing unprecedentedly fast progress in recent years. [17-20]

In this review paper, we introduce recent progress in the field of hybrid energy harvesting, largely focusing on the solar cell and mechanical energy harvester. First, a basic theory and mechanism of each device is explained, and then we expand our focus to an integrated energy harvester. Second, we introduce piezotronics and piezo-phototronics for a hybrid energy harvester, combining two different physical effects, such as a photovoltaic and piezoelectric effect. Mechanisms of the piezotronics and piezo-phototronics are explained, which is followed by theoretical studies and demonstration of the device applications. For all hybrid energy harvesting applications, we particularly focus on

[a] Dr. Yuljae Cho
     Department of Engineering Science, University of Oxford
     Parks Road, Oxford OX1 3PJ, United Kingdom

[b] Dr. Sangyeon Pak and Prof. SeungNam Cha
     Department of Physics, Sungkyunkwan University
     Suwon, Republic of Korea
     e-mail: chasn@skku.edu

[c] Prof. Geon-Hyoung An
     Department of Energy Engineering, Gyeongnam National University of Science and Technology
     Jinju-si, Geyongsangnam-do 52725, Republic of Korea

[d] Dr. Bo Hou
     Department of Engineering, University of Cambridge
     9 JJ Thomson Avenue, Cambridge CB3 0FA, United Kingdom
     e-mail: bh478@cam.ac.uk

colloidal quantum dots (QDs) as they possess fascinating material properties for solar energy harvesting, such as (1) bandgap tunability by engineering the size of nanocrystals, (2) high absorption coefficient, and (3) solution processability, enabling facile material deposition technique as shown in Figure 1, which is universal phenomena for various kinds of QDs, for example Cd-based,[21-23] Pb-based,[24-29] and recently developed perovskite QDs.[30-33]
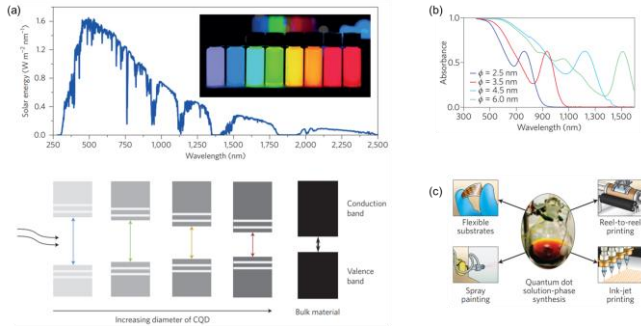

Figure 1. (a) Bandgap tunability by engineering the size of QD nanocrystals. The inset illustrates the photoluminescence of QDs concerning crystal sizes. Reprinted from reference 34 with permission. Copyright 2016, Springer Nature. (b) An example of the absorption spectrum of a QD solution where ϕ indicates the Bohr exciton radius. (c) Various colloidal QD deposition techniques, such as spray, reel-to-reel, and ink-jet printing for a flexible QD solar cell application. Reprinted from reference 35 with permission. Copyright 2012, Springer Nature.

2. Integration of a quantum dot solar cell for a hybrid energy harvester

2.1. Mechanism of a QD solar cell

Researches on a solar cell date back to late 19th century when the first solar cell was invented using the photovoltaic effect. Then, half of century later, the first commercialized solar cell was produced at Bell Labs. Nowadays, solar cell research is one of the major research topics in the interdisciplinary field. Among various materials for solar cell applications, QDs have attracted great interest for solar cell applications because of their excellent properties such as tunability of bandgap, quantum confinement, high light absorption coefficient, and solution processability.[29,36]

When a solar cell absorbs light, an electron-hole pair (exciton) is generated by a photovoltaic effect. Then, the photo-generated electron and hole pair is dissociated into an electron and a hole which are collected at electrodes.[37] Collection of charges at the electrodes generates current (I) which can be described as an equation (1) below.

$$I = I_s\left(e^{V_a/V_t} - 1\right) - I_{ph} \quad (1)$$

where Is is the dark saturation current, Va is the applied bias, and V_t is the thermal voltage (typically kT/q).[37] Short circuit current (I_{SC}) of a solar cell refers to a current generated by a solar cell at zero voltage bias. Meanwhile, an open circuit voltage is where a current of a solar cell crosses a value of zero on the x-axis, i.e. I = 0, which can be described as an equation (2).

$$\begin{cases} I = 0 \text{ and thus } I_S\left(e^{V_a/V_t} - 1\right) - I_{ph} = 0 \\ V_a = V_t \ln\left(\frac{I_{ph}}{I_s} + 1\right) = V_{oc} \end{cases} \quad (2)$$

Because the power of a device is a product of current and voltage, the output power of a solar cell is simply calculated by an equation (3).

$$P = I \times V_a = I_s V_a\left(e^{v_a/v_t} - 1\right) - I_{ph}V_a \quad (3)$$

Then, by using the first-order differential, the maximum power can be calculated, from which the fill factor (FF) of a solar cell can be obtained which is the ratio between the maximum power and the theoretical power ($P_t = I_{sc} \times V_{oc}$) as the equation (4) describes.

$$FF = \frac{P_{max}}{P_t} = \frac{I_{max}V_{max}}{I_{sc}V_{oc}} \quad (4)$$

Using solar cell parameters obtained from the equations (1), (2), and (4), a power conversion efficiency of a solar cell is obtained (equation (5) where P_{in} is the incident light power, Air Mass (AM) 1.5G, i.e., 1 sun, (100 mWcm⁻²).[37,38]

$$PCE = \frac{P_{out}}{P_{in}} = FF\frac{I_{sc}V_{oc}}{P_{in}} \quad (5)$$
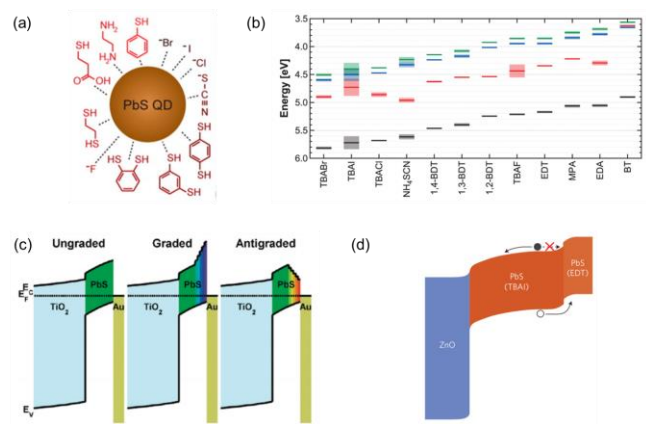

Figure 2. (a) Illustration of organic and inorganic ligands of QDs (b) Energy level diagrams of PbS QDs treated by different kinds of ligands. QDs used in the figure have approximately 1.3 eV bandgap. Reprinted from reference 39 with permission. Copyright 2014, American Chemical Society. (c) Schematics of a QD solar cell structure employing ungraded, graded and antigraded junction. Reprinted from reference 40 with permission. Copyright 2011, American Chemical Society. (d) An example of a graded junction using two different ligands with a structure of ZnO/PbS-TBAI/PbS-EDT. Reprinted from reference 41 with permission. Copyright 2014, Springer Nature.

Generally, colloidal QDs are capped with ligands consisting of a long carbon chain, such as oleic acid (OA) and oleylamine (OLA) to stabilize them in a solution phase. Due to the long chain ligands, however, the freshly synthesized QDs have poor electric conductivity. Therefore, the functionalization of QDs using short chain ligands is required for electronic/optoelectronic applications (Figure 2(a)). Figure 2(b) describes energy levels of a QD layer treated by each ligand, which is resulted from the sum of the dipole moment induced by interaction between the surface of QD and binding ligand, and intrinsic dipole moment of the ligand.[39] The energy level difference in a QD film can be judiciously used to form a graded junction structure in order to facilitate charge transport as shown in Figure 2(c).[40] Using this strategy in Figure 2(d), Chuang et al. demonstrated the significantly improved performance of a QD solar cell and its stability up to 150 days in ambient air.[41]

2

2.2. Mechanism of mechanical energy harvester

Mechanical energy sources which are generally in the form of vibrations, such as sound and wind, are ubiquitous and bountiful in our daily lives. Unlike solar power, mechanical energy sources are not dependent on the time and region. However, unfortunately, most of the mechanical energy sources are wasted because of the lack of abilities to harvest these energy sources. In 2006, the first piezoelectric nanogenerator (PENG) was invented using a piezoelectric effect of ZnO nanowire arrays, which demonstrated that wasted energy could be converted into useful electrical energy.[1] Ever since the first invention of a PENG, this area has attracted tremendous research interest.[1,42-44] Furthermore, in 2012, Fan et al. introduced a triboelectric nanogenerator (TENG) for the first time, which is based on the contact electrification.[4]
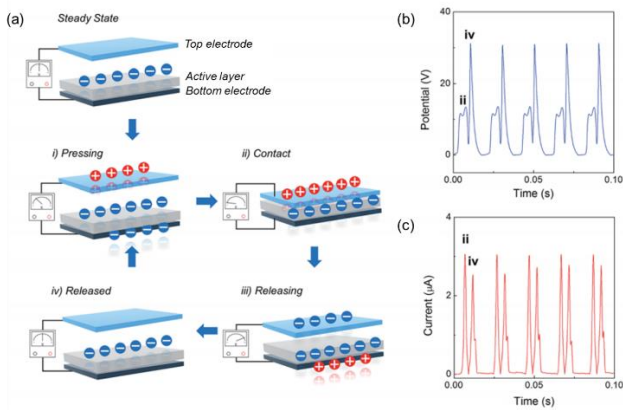

Figure 3. (a) An illustration of the operating principle of a mechanical energy harvester. Output characteristics of a mechanical energy harvester; (b) Potential and (c) current, driven at a frequency of 50 Hz. Reprinted from reference 17 with permission. Copyright 2018, Royal Society of Chemistry.

Figure 3 shows a mechanism of the mechanical energy harvesting processes where we assume that an active layer has negative surface charges. It is worth noting that for negative and positive surface charges the mechanism is still the same except for that charge polarity is opposite to Figure 3(a). Triboelectric series can be found in reference 45 and 46. Due to the negative surface charges, positive charges are induced to the top electrode when the top electrode is approaching the active layer. This again leads to induce negative charges at the bottom electrode (Figure 3(a)-(i)). Then, electrons induced at the bottom electrode are transported to the top electrode to neutralize electric potential difference between the two electrodes (Figure 3(a)-(ii)). On the contrary, when the pressure is realized, electrons on the top electrode move back to the bottom electrode to neutralize the potential difference which was caused by transport of electrons to the top electrodes (Figure 3(a)-(iii)).[47-49] Figure 3(b) and (c) illustrate rectified potential and current output characteristics of the mechanical energy harvester at the input frequency of 50 Hz, respectively. Governing equations for each a piezoelectric or triboelectric effect are described below.

$$\nabla E = {}^{\rho}/_{\varepsilon}, \ \rho = d_{ij}X \text{ for a piezoelectric harvester (6)}$$

$$V = {}^{-\rho d}/_{\varepsilon_0} \text{ for a triboelectric harvester (7)}$$

where ρ is the polarization charge density, ε is the dielectric permittivity, d_{ij} is the piezoelectric coefficient, X is the applied stress, d is an interlayer distance, and ε_0 is the vacuum permittivity.[12] As both equations describe, basically a potential generated by a mechanical energy harvester is a function of the charge density (ρ). The difference between a PENG and TENG is that a potential of the TENG is also a function of an interlayer distance (d). This is because the piezoelectric charges are related to the crystal structure whereas the triboelectric charges are associated with the contact electrification effect. The typical materials for a mechanical energy harvester are ZnO nanowires, PbZrTiO, BaTiO, and poly(vinylidene fluoride) (PVDF)-based polymers for a PENG,[45-49->50-54] and PTFE, PDMS, and PVDF-based polymers for a TENG.[55-59]

2.3. Hybrid energy harvesting device

Mechanisms of energy harvesting involving photovoltaic, piezoelectric and triboelectric effects are discussed in the previous section. An energy harvester harnessing each phenomenon has demonstrated fascinating device performances. However, the energy harvesting device involving only one physical effect mentioned above is susceptible to suffer from interruption of power supply due to the intermittency of environmental energy sources, such as sunlight, wind, and mechanical vibrations. Moreover, high contrast in output characteristics of different types of energy harvesters was observed; for example, a PENG and TENG typically have high voltage whereas low current output where a solar cell exhibits an opposite characteristic to a PENG and TENG.[47,60] The high contrast of output performance suggests that a hybrid energy harvester is highly desirable to achieve a high current from one harvester while enhancing a potential limit from the other. Furthermore, hybridized energy harvesting can harness various kinds of environmental energy sources simultaneously. This significantly reduces sudden power interruption caused by intermittence of environmental energy.[47,61]

In this regard, hybrid energy harvesting is one of the potential approaches to overcome limitations that an energy harvesting device is harnessing a particular environmental energy source, which ultimately realizes sustainable power supply to sensor networks for the Internet of Things (IoT). In this section, we review a hybrid energy harvesting technology involving a QD photovoltaic and piezo/triboelectric device.

A hybrid energy harvester which can simultaneously harness mechanical vibrations and photons has been intensively researched after the first demonstration by Wang's group in 2009.[62] This hybrid energy harvester typically consists of a mechanical energy harvester (PENG or TENG) and a solar cell. As shown in Figure 4, all different kinds of solar cells, such as a dye-sensitized solar cell (DSSC), quantum dots, silicon (Si), and organic-inorganic hybrid solar cells, successfully demonstrated the integration with a mechanical energy harvester.[63-66] Here, we focus more on a hybrid energy harvester with a QD-based solar cell.
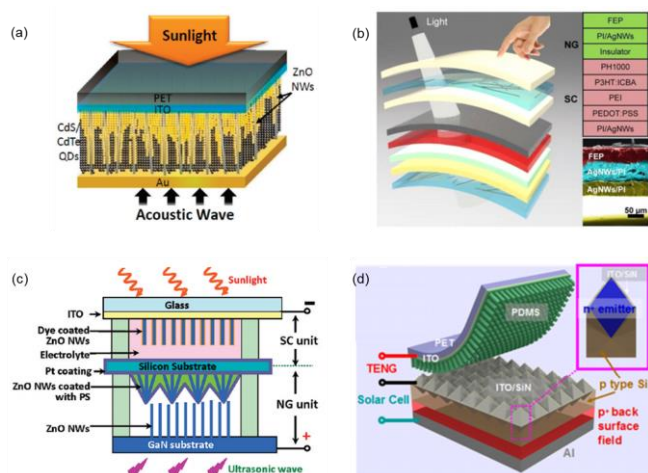
Figure 4. Schematics of hybrid energy harvesters consisted of a mechanical energy harvester and a solar cell using different kinds of materials, such as (a) CdS/CdTe QDs (Reprinted from reference 64 with permission. Copyright 2010, American Chemical Society), (b) polymer (Reprinted from reference 65 with permission. Copyright 2009, American Chemical Society), (c) dye-sensitizer (Reprinted from reference 62 with permission. Copyright 2015, Elsevier), and (d) silicon (Reprinted from reference 66 with permission. Copyright 2013, American Chemical Society).

In 2010, Lee et al. reported a hybrid energy harvester based on ZnO NWs and infiltrated CdS/CdTe QDs among vertical structure ZnO NW. The harvester was driven by acoustic vibrations, of which working range was 35 – 1000 Hz.[64] However, output performances of the hybrid energy harvester were relatively low to power electronic devices. Meanwhile, an invention of a TENG in 2012 significantly enhanced an output performance of a mechanical energy harvester, which spurred tremendous research interests in a hybrid energy harvester as well.[4,67,68]

Using a TENG, in 2018, Cho *et al*. reported a hybrid TENG and a PbS QDSC energy harvester for a reliable and sustainable sensor system to realize IoT technology as the IoT is a prerequisite condition in the era of smart life which will enrich lives of human beings in the near future.[17] This work suggested two possible routes to enhance the overall performance of the hybrid energy harvester: (1) By employing a highly transparent P(VDF-TrFE-CTFE) (full name) and graphene electrode, the hybrid energy harvester maximized absorption of sunlight coming to PbS QD layers as shown in Figure 5(a); (2) In order to increase V_{oc} of a solar cell, six patterned ITOs connected in series were used as shown in Figure 5(b). Circuit design to integrate two distinct signals, direct current from a PbS QD solar cell and alternative current from a TENG, is also shown at the bottom of Figure 5(b). The energy harvester demonstrated dual mode and simultaneous energy harvesting with respect to input energy sources: photons (i), both photons and vibrations (ii), and vibrations (iii) as shown in Figure 5(c). Accordingly, capacitor charging rates with respect to the input energy sources were investigated. Figure 5(d) shows the complimentary and synergetic effects of a hybrid system. The potential in an external capacitor was charged approximately to 2.6, 7.5 and 11 V for photons, vibrations, and both, respectively.

In addition, the calculated charging rate was found to be 14, 40, and 58 mV sec^{-1} for photons, vibrations, and both, respectively. Lastly, the author demonstrated an operation of an IR sensor powered only by the hybrid energy harvester as shown in Figure 5(e) and (f), suggesting that the hybrid energy harvester can be used as a stable power supply to realize IoT technology.
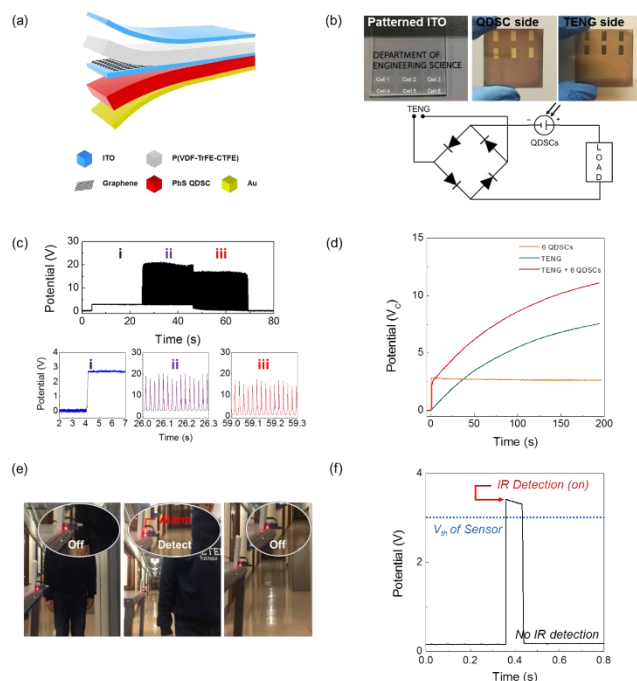
Figure 5. (a) Illustration of a hybrid energy harvester. (b) Pictures on top show a patterned ITO electrode (left), a fabricated QDSC (middle), and a TENG (right). A bottom image shows an integration circuit for a hybrid energy harvester. (c) Performances of the hybrid energy harvester with respect to input signals. (d) Potential in an external capacitor charged by photons (yellow), mechanical vibrations (green), and both photons and vibrations simultaneously (red). (e) An IR sensor powered by a hybrid energy harvester. (f) Operation of the IR sensor when IR was detected. Reprinted from reference 17 with permission. Copyright 2018, Royal Society of Chemistry.

In this section, we reviewed hybrid energy harvesting technology with a QDSC and a mechanical energy harvester. Hybridization of different types of energy harvesters enables simultaneous energy harvesting from various kinds of input energies, such as solar power and mechanical vibrations. This method mitigates and resolves sudden power interruption due to intermittence of energy from nature.

3. Piezotronic and piezo-phototronic effect on a quantum dot solar cell

Photon energy harvesting has attracted tremendous research interests for many decades. However, current solar cell technology, whether it is a commercialized or laboratory photovoltaic cell, has not yet achieved PCE over the Schockley-Queisser limit, i.e. the detailed balance limit. One of the reasons for the below theoretical limit stems from inherent material properties, for example mid-band gap states, defects, and non-ideal interfaces. One possible route to overcome the inherent

material-related limitations is the introduction of an additional electric potential on top of a built-in potential at a semiconductor junction, and this can be achieved through a strain-induced piezoelectric charge/potential. This additional piezoelectric potential prevents loss of charges prior to recombination at the defect sites.[25,27,69] In this section, we review the mechanism and theoretical backgrounds of piezotronics as well as piezo-phototronics and discuss a potential route towards enhancing the solar cell efficiency using a piezo-phototronic effect. An additional electric field that was induced by a piezoelectric was found to be able to modify the properties at an interface between a piezoelectric layer and photo-active layer.

3.1. Piezotronic and Piezo-phototronic mechanism

3.1.1. Piezotronics

A piezotronics introduced by Zhong Lin Wang in 2006 explains piezoelectric properties of a semiconductor. This phenomenon generally occurs at an interface between a piezoelectric semiconductor and metal/semiconductor.[70-72] Through strain engineering, local band structure and/or band alignment can be modulated, which consequently tunes junction properties. Since the first demonstration of the piezotronics, it has attracted tremendous research interests from interdisciplinary areas such as electronics, optoelectronics, and electrochemistry.[73-81]
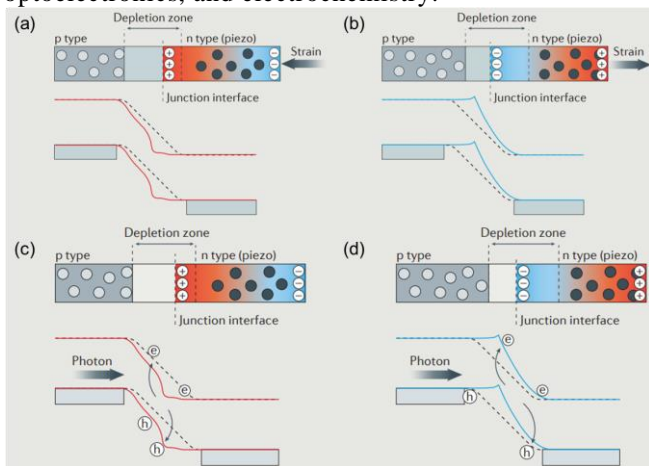
Figure 6. Illustrating mechanisms of (a), (b) a piezotronics effect, and (c), (d) a piezo-phototronic effect. Reprinted from reference 70 with permission. Copyright 2016, Springer Nature.

A mechanism of the piezotronics effect is illustrated in Figure 6(a) and (b). Upon application of strain, a piezoelectric material produces polarization charges due to deformation of a crystal structure. The polarized charges lead to retribution of free charges, which results in a modulation of energy band structure at the interface. For example, when positive charges are induced at the interface between an n-type piezoelectric material and a p-type semiconductor (Figure 6(c)), a depletion width on n-type decreases whereas a depletion width on p-type increases. As the depletion region on the n-type side becomes much narrower, a local band structure is changed due to the positive polarized charges at the interface. The opposite phenomena can be observed when

negative polarization is induced at the interface as shown in Figure 6(b).

3.2.2. Piezo-phototronics

The piezo-phototronic effect refers to the coupling of piezoelectricity, optical processes, and charge transport in semiconductors to modulate characteristics of charge carrier behaviors in optoelectronic devices.[65,66] It was first reported in 2010 in a metal-ZnO NWs system with an observation of the coupling between piezoelectricity and photoexcitation.[82-84] The Schottky barrier height was modulated by the coupling effect, which resulted in engineering optoelectronic processes.[82,83] Ever since the first demonstration of the piezo-phototronic effect, tremendous experimental studies were carried out for various optoelectronic devices, such as photodetectors, solar cells, and light-emitting diodes (LEDs), while theoretical studies were performed to support experimental results.[85-93]

Mechanism of a piezo-phototronic effect is shown in Figure 6(c) and (d). Similar to the piezotronics effect, local energy band is modulated with respect to induced piezoelectric charge/potential at the interface between an n-type piezoelectric material and a p-type semiconductor. This modulated local energy band changes behavior of electron-hole pairs generated by a photonic effect. For example, when positive charges are induced at the interface a depletion width and accordingly a local band structure is modified as explained in the piezotronics effect (Figure 6(c)). This results in less effective charge separation and thus deterioration of device performance. In contrast, when negative charges are induced at the junction a depletion width increases on the n-type piezoelectric material, which reduces the effective series resistance and consequently charge injection is facilitated (Figure 6(d)). As a result, non-radiative recombination is suppressed, which results in improvement in device performance.

3.2. Theoretical analysis of piezo-phototronic effect on solar cells

Prior to review piezo-phototronic effect on a solar cell, first a basic theory of the piezo-phototronic will be discussed. The core idea of the piezo-phototronic effect on a solar cell is that it uses an additional piezoelectric potential/field generated by strain/stress in order to improve charge extraction and exciton dissociation, which results in increase in the overall performance of a solar cell.[18] Deep theoretical studies were performed by Zhang et al. by using a typical n-type piezoelectric ZnO NWs and p-type non-piezoelectric material.[92] Assuming that J_{SC} is free from stress/strain, photocurrent of a solar cell with a piezoelectric effect can be written as the equation (8) below, where ρ_{piezo} is the density of piezoelectric charges, W_{piezo} is the width of the created piezoelectric charge zone.[88,94,95]

$$J = J_{pn0} \cdot \exp\left[-q^2 \rho_{piezo} W^2 (2kT\epsilon_s)^{-1}\right] \left[\exp\left(\frac{qV}{kT}\right) - 1\right] - J_{SC} \quad (8)$$

$$\text{where } J_{pn} = J_{pn0} \cdot \exp\left[-q^2 \rho_{piezo} W^2 (2kT\epsilon_s)^{-1}\right]$$

From the equation (8), V_{oc} can be obtained by assuming J = 0. Then, V_{oc} of a solar cell with a piezoelectric effect can be written as the equation (9).

5

$$V_{OC} = \frac{kT}{q} \cdot \ln\left(\frac{J_{SC}}{J_{pn}} + 1\right) \quad (9)$$

V_{oc} of a solar cell can be re-written as the equation (10) by assuming that $J_{SC} \gg J_{pn}$, which holds for a typical solar cell.[94,95]

$$V_{OC} \approx \frac{kT}{q} \cdot \ln\left(\frac{J_{solar}}{J_{pn}}\right) = \frac{kT}{q} \cdot \left[\ln\left(\frac{J_{solar}}{J_{pn0}}\right) + q^2 \rho_{piezo} W^2 (2kT\epsilon_s)^{-1}\right] \quad (10)$$

The equation (10) describes that piezoelectric charge through the application of strain/stress is one of the key parameters that determine V_{oc} of a solar cell as shown in Figure 7(a) and (b). This mechanism also holds for a case of an n-type non-piezoelectric material and a p-type piezoelectric material as shown in Figure 7(c) and (d). More details about theoretical studies of piezo-phototronic effect on a solar cell can be found in numerous references.[96-98]
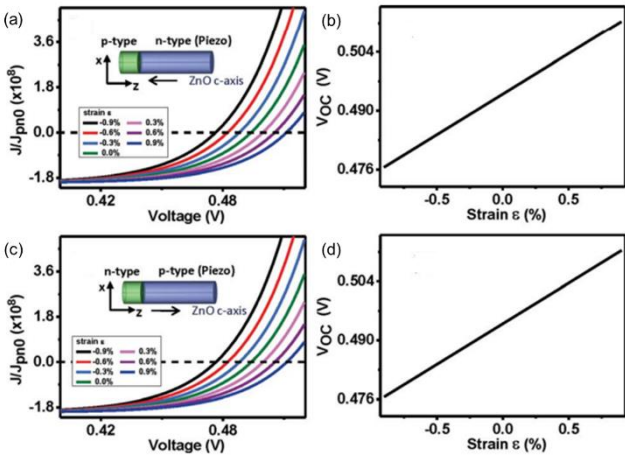
Figure 7. (a) Current curves as a function of voltage and (b) modulation of open circuit voltage with respect to applied strains (0.9% to 0.9%) where an n-type material is a piezoelectric semiconductor. (c) Current curves as a function of voltage and (d) modulation of open circuit voltage with respect to applied strains (0.9% to 0.9%) where a p-type material is a piezoelectric semiconductor. Reprinted from reference 92 with permission. Copyright 2012, Royal Society of Chemistry.

3.3. Experimental demonstrations of piezo-phototronic effect on quantum dot solar cells

Along with the theoretical studies, a number of experimental studies demonstrate the piezo-phototronic effect on charge carrier characteristics and performances of a solar cell.[88,95,99-103] The experimental results are consistent with the theoretical analysis in the previous section. Demonstrations of piezo-phototronic effect on solar cells have been made in various photoactive materials, such as quantum dots, nanowires, and organic/polymers. Here, we focus on the piezo-phototronic effect on QD solar cells (QDSCs), in particular.

3.3.1. Depletion-heterojunction QDSCs

Piezoelectric-polarization-enhanced depletion-heterojunction QDSCs (DH QDSC) has demonstrated by Shi et al. in 2013.[90] Piezocharges between (0001)-oriented texture ZnO film and p-type 1,2-ethanedithiol (EDT)-treated PbS QDs layers were induced by an

application of strains to a QDSC. Accordingly, interfacial energy band at the junction between ZnO-PbS QDs was modulated by piezoelectric potential (P_{PZ}), which led to modulation of PCE. The working mechanism of piezoelectric-polarization-enhanced depletion-heterojunction QDSCs is shown in Figure 8(a)-(d). When positive P_{PZ} is generated at the interface, a depletion width in PbS layers increased whereas a deletion width in a ZnO layer became narrower Figure 8(a) and (c). Because the electron mobility of p-type PbS QDs is slower than that of a n-type ZnO layer, charge extraction is facilitated, resulting in enhanced solar cell performance. On the contrary, when negative PPZ is induced at the interface, a band offset is reduced to $\emptyset_{bi,PbS} - \Delta\emptyset_{PZ,PbS}$ and the depletion region in the PbS layers decreased ($\delta_{PZ,PbS} < \delta_{0,PbS}$) as shown in Figure 8(b) and (d). Therefore, overall charge extraction at the junction is aggravated, resulting in a poor solar cell performance.
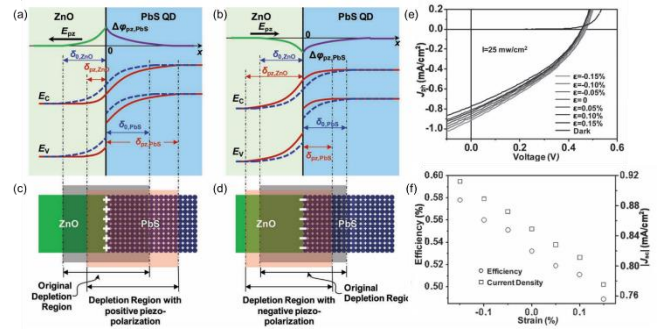

Figure 8. Schematics of QDSC energy band diagram with (a) positive and (b) negative piezocharges at the ZnO/PbS QDs interface, respectively. Schematics of changes of depletion region with respect to (c) positive and (d) negative piezocharges at the ZnO/PbS interface, respectively. (e) Photocurrent curves as a function of the potential of a ZnO/PbS QDSC under different strains applied. (f) Conversion efficiency and short circuit current as a function of applied strain to the device. Reprinted from reference 90 with permission. Copyright 2013, John Wiley and Sons.

As shown in Figure 8(e) and (f), performances of QDSCs under an illumination intensity of 25 mWcm^{-2} are modulated with respect to the strain applied. The efficiency was modulated from 0.51 to 0.55 %, changing rate for 0.01 % strain, respectively. Under an illumination intensity of 0.0047 mWcm^{-2}, QDSCs exhibited a much higher rate of J_{SC} and PCE modulation, for example, increase in J_{SC} was from approximately 1.5 to 2.5 µA cm^{-2} and improvement in PCE was from 3.1 to 4.0 %, respectively. The piezo-phototronic effect assisted J_{SC} and PCE modulation strategy using P_{PZ} gives a new insight into the improvement of charge carrier extraction and transport in DH QDCSs.

3.3.2. An inverted structure flexible PbS QDSC

Inverted PbS QDSC structure was introduced by Chuang et al. in 2014.[41] By forming a QD junction between tetrabutylammonium iodide (TBAI)- and 1,2-ethanedithiol (EDT)-treated PbS QD layers, significantly improved performance and stability of QDSCs were achieved. However, a heterojunction between electron transport ZnO and QD layers still need to be improved to enhance the performance of QDSCs. In particular, a flexible QDSC suffers severely from charge carrier loss

6

at the heterojunction because of defects and traps that arise from the straining of semiconducting layers during fabrication and measurement processes. This recombination pathway needs to be resolved to improve the performance of a flexible QDSC.[104,105]
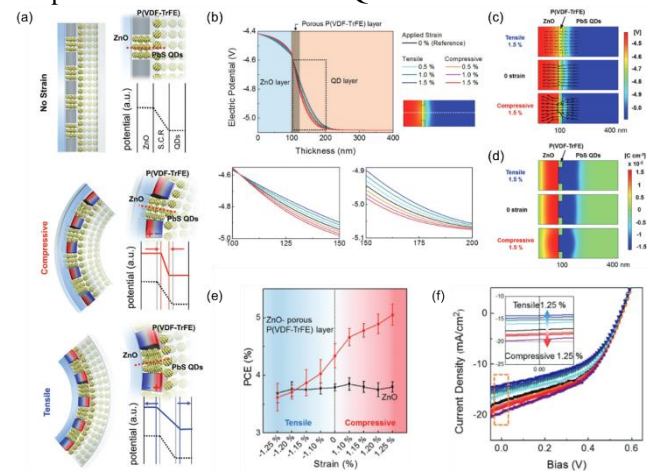

Figure 9. (a) Schematics of the junction property modulation concerning the strain applied; no strain, the application of a compressive and a tensile strain. (b)-(d) Simulation results to demonstrate modulation of junction properties upon the application of a compressive and tensile strain. (e) Modulation of the PCE with respect to the application of a tensile and compressive strain. (f) Photocurrent curves as a function of applied bias at no strain and with strain ranging from -1.25 to 1.25%; top left inset shows enlarged J_{SC} at different strain rates. Reprinted from reference 18 with permission. Copyright 2018, John Wiley and Sons.

Recently, Cho et al. employed a porous structure of piezoelectric poly(vinylidenefluoride-trifluoroethylene) (P(VDF-TrFE)) layer at the interface between ZnO and QD layers to facilitate extraction and reduce the recombination of charge carriers.[18] A piezoelectric potential generated by the inserted porous P(VDF-TrFE) layer at the heterojunction consequently changed the charge transport behavior through the addition a piezoelectric potential. Figure 9(a) illustrates schematics of the modulation in the heterostructure properties with respect to applied strain; (a) no strain, (b) a compressive and (c) a tensile strain. S.C.R in the figure indicates a space charge region. The modulation of the potential profile at the junction described in the schematics was demonstrated by using COMSOL simulation as shown in Figure 9(b)-(d). Basically, an electric potential/field at the heterojunction increased upon the application of compressive strain (Figure 9(b) and (c)). This is because a depletion width is reduced when compressive strain is applied, which resulted in the formation of a higher electric field across the junction (Figure 9(c) and (d)). Attributed to an additional piezoelectric potential at the junction, the performance of the flexible QDSC was able to be actively modulated by applying various strain rates. Using this approach, PCE of a flexible QDSC was enhanced up to 37%.

4. Conclusion and outlook

In conclusion, we summarized the recent progress in hybrid energy harvesting technology, particularly considering the solar cell and mechanical energy harvester. Significant progress has been made in the field of energy harvesting for several decades. However, there are still challenges in the development of sustainable energy harvesting devices because environmental energy is intermittent by nature. Therefore, two approaches to realize a hybrid system has been introduced (Figure 10); (1) integration of a solar cell and mechanical energy harvester and (2) utilization of a piezotronic/ piezo-phototronic effect. Throughout the review, we particularly focus on QDs for a hybrid energy harvesting device due to their unique and excellent material properties for energy harvesting. At last, a summary and perspectives for practical guidelines are provided.
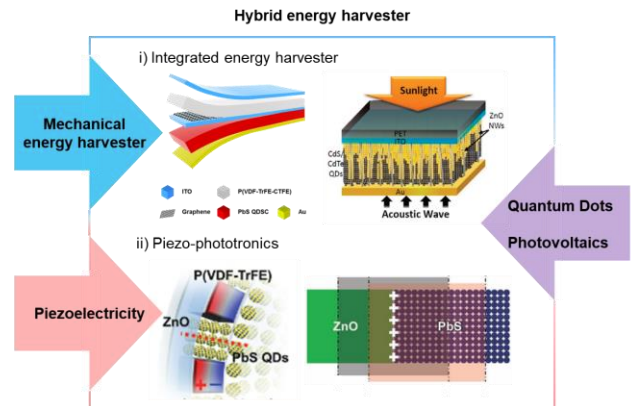

Figure 10. A hybrid energy harvesting system; (i) an integration of a solar cell and mechanical energy harvester and (ii) utilization of a piezo-phototronic effect. Reprinted from references (i) 17 and 64 with permission. Copyright 2018, Royal Society of Chemistry and Copyright 2010, American Chemical Society, respectively. Reprinted from references (ii) 18 and 90 with permission. Copyright 2018 and 2013, respectively, John Wiley and Sons.

First, background as well as basic mechanism of the QD solar cell and mechanical energy harvester (a PENG and TENG) was described, which was followed by an introduction of recent advancement in an integration technology of the solar cell and mechanical energy harvester. The hybrid device is benefited from simultaneous energy harvesting of different kinds of environmental energy sources, which greatly enhance stability and sustainability of the device from sudden power interruption. In addition, a potential application of a hybrid energy harvester as a stable power supply for IoT technology has been demonstrated.

Second, a number of studies to combine two different physical effects, namely a photovoltaic and piezoelectric effect, was reviewed with the explanation on mechanisms of the piezotronics, piezo-phototronics, and their theories. To overcome intrinsic material properties, such as mid-band gap states and defects, a strain-induced piezoelectric potential was judiciously introduced at a junction interface, which leads to the modulation of the junction properties and eventually significant enhancement in the performance of the solar cell. We believe that this review suggests a guideline for future energy harvesting technology involving a photovoltaic and piezo/triboelectric effect.

Acknowledgements

References

[1] Z. L. Wang, J. Song, *Science* **2006**, *312*, 242-246.

[2] W. Wu, L. Wang, Y. Li, F. Zhang, L. Lin, S. Niu, D. Chenet, X. Zhang, Y. Hao, T. F. Heinz, *Nature* **2014**, *514*, 470-474.

[3] S. Xu, Y. Qin, C. Xu, Y. Wei, R. Yang, Z. L. Wang, *Nat. Nanotechnol.* **2010**, *5*, 366-373.

[4] F. Fan, Z. Tian, Z. L. Wang, *Nano Energy* **2012**, *1*, 328-334.

[5] G. Zhu, J. Chen, T. Zhang, Q. Jing, Z. L. Wang, *Nat. Commun.* **2014**, *5*, 3426.

[6] Q. Jing, Y. Xie, G. Zhu, R. P. Han, Z. L. Wang, *Nat. Commun.* **2015**, *6*, 8031.

[7] B. O'regan, M. Grätzel, *Nature.* **1991**, *353*, 737-740.

[8] P. Wang, S. M. Zakeeruddin, J. E. Moser, M. K. Nazeeruddin, T. Sekiguchi, M. Grätzel, *Nat. Mater.* **2003**, *2*(6), 402-407.

[9] J. You, L. Dou, K. Yoshimura, T. Kato, K. Ohya, T. Moriarty, K. Emery, C. Chen, J. Gao, G. Li, *Nat. Commun.* **2013**, *4*, 1446.

[10] J. Jean, P. R. Brown, R. L. Jaffe, T. Buonassisi, V. Bulović, *Energy Environ. Sci.* **2015**, *8*, 1200-1219.

[11] B. Parida, S. Iniyan, R. Goic, *Renew. Sustainable Energy Rev.* **2011**, *15*, 1625-1636.

[12] J. Lee, J. Kim, T. Y. Kim, M. S. Al Hossain, S. Kim, J. H. Kim, *J. Mater. Chem. A* **2016**, *4*, 7983-7999.

[13] W. Li, D. Torres, R. Díaz, Z. Wang, C. Wu, C. Wang, Z. L. Wang, N. Sepúlveda, *Nat. Commun.* **2017**, *8*, 15310.

[14] J. Wang, S. Li, F. Yi, Y. Zi, J. Lin, X. Wang, Y. Xu, Z. L. Wang, *Nat. Commun.* **2016**, *7*, 12744.

[15] J. Chen, Y. Huang, N. Zhang, H. Zou, R. Liu, C. Tao, X. Fan, Z. L. Wang, *Nat. Energy.* **2016**, *1*, 16138.

[16] K. Song, J. H. Han, T. Lim, N. Kim, S. Shin, J. Kim, H. Choo, S. Jeong, Y. Kim, Z. L. Wang, *Adv. Healthcare Mater.* **2016**, *5*, 1572-1580.

[17] Y. Cho, S. Lee, J. Hong, S. Pak, B. Hou, Y. Lee, J. E. Jang, H. Im, J. I. Sohn, S. Cha, J. M. Kim, *J. Mater. Chem. A* **2018**, *6*, 12440-12446.

[18] Y. Cho, P. Giraud, B. Hou, Y. Lee, J. Hong, S. Lee, S. Pak, J. Lee, J. E. Jang, S. M. Morris, J. I. Sohn, S. Cha, J. M. Kim, *Adv. Energy Mater.* **2018**, *8*, 1700809.

[19] Q. Lai L. Zhu Y. Pang, L. Xu, J. Chen, Z. Ren, J. Luo, L. Wang, L. Chen, K. Han, P. Lin, D. Li, S. Lin, B. Chen, C. Pan, Z. L. Wang, *ACS Nano* **2018**, *12*, 10501-10508.

[20] Z. L. Wang, *Nano Energy* **2018**, *54*, 477-483.

[21] T. Shu, Z. Zhou, H. Wang, G. Liu, P. Xiang, Y. Rong, H. Han, Y. Zhao, *J. Mater. Chem.* **2012**, *22*, 10525-10529.

[22] Z. Pan, K. Zhao, J. Wang, H. Zhang, Y. Feng, X. Zhong, *ACS Nano.* **2013**, *7*, 5215-5222.

[23] Y. Justo, P. Geiregat, K. Van Hoecke, F. Vanhaecke, C. De Mello Donega, Z. Hens, *J. Phys. Chem. C* **2013**, *117*, 20171-20177.

[24] B. Kim, D. C. Neo, B. Hou, J. B. Park, Y. Cho, N. Zhang, J. Hong, S. Pak, S. Lee, J. I. Sohn, H. E. Assender, A. AR. Watt, S. Cha, J. M. Kim, *ACS Appl. Mater. Interfaces* **2016**, *8*, 13902-13908.

[25] B. Hou, Y. Cho, B. S. Kim, J. Hong, J. B. Park, S. J. Ahn, J. I. Sohn, S. Cha, J. M. Kim, *ACS Energy Lett.* **2016**, *1*, 834-839.

[26] J. Hong, B. Hou, J. Lim, S. Pak, B. Kim, Y. Cho, J. Lee, Y. Lee, P. Giraud, S. Lee, J. B. Park, S. M. Morris, H. J. Snaith, J. I. Sohn, S. Cha, J. M. Kim, *J. Mater. Chem. A* **2016**, *4*, 18769-18775.

[27] Y. Cho, B. Hou, J. Lim, S. Lee, S. Pak, J. Hong, P. Giraud, A. Jang, Y. Lee, J. Lee, J. E. Jang, H. J. Snaith, S. M. Morris, J. I. Sohn, S. Cha, J. M. Kim, *ACS Energy Lett.* **2018**, *3*, 1036-1043.

[28] B. Kim, J. Hong, B. Hou, Y. Cho, J. I. Sohn, S. Cha, J. M. Kim, *Appl. Phys. Lett.* **2016**, *109*, 063901.

[29] B. Hou, Y. Cho, B. Kim, D. Ahn, S. Lee, J. B. Park, Y. Lee, J. Hong, H. Im, S. M. Morris, J. I. Sohn, S. Cha, J. M. Kim, *J. Mater. Chem. C* **2017**, *5*, 3692-3698.

[30] L. M. Wheeler, E. M. Sanehira, A. R. Marshall, P. Schulz, M. Suri, N. C. Anderson, J. A. Christians, D. Nordlund, D. Sokaras, T. Kroll, S. P. Harvey, J. J. Berry, L. Y. Lin, J. M. Luther, *J. Am. Chem. Soc.* **2018**, *140*, 10504-10513.

[31] J. Xue, J. Lee, Z. Dai, R. Wang, S. Nuryyeva, M. E. Liao, S. Chang, L. Meng, D. Meng, P. Sun, O. Lin, M. S. Goorsky, Y. Yang, *Joule* **2018**, *2*, 1866-1878.

[32] Z. Zolfaghari, E. Hassanabadi, D. Pitarch-Tena, S. J. Yoon, Z. Shariatinia, J. van de Lagemaat, J. M. Luther, I. Mora-Seró, *ACS Energy Lett.* **2018**, *4*, 251-258.

[33] A. Hazarika, Q. Zhao, E. A. Gaulding, J. A. Christians, B. Dou, A. R. Marshall, T. Moot, J. J. Berry, J. C. Johnson, J. M. Luther, *ACS Nano* **2018**, *12*, 10327-10337.

[34] M. Yuan, M. Liu, E. H. Sargent, *Nat. Energy* **2016**, *1*, 16016.

[35] E. H. Sargent, *Nat. Photon.* **2012**, *6*, 133-135.

[36] S. Pak, Y. Cho, J. Hong, J. Lee, S. Lee, B. Hou, G. An, Y. Lee, J. E. Jang, H. Im, S. M. Morris, J. I. Sohn, S. Cha, J. M. Kim, *ACS Appl. Mater. Interfaces* **2018**, *10*, 38264–38271.

[37] A. Luque, S. Hegedus, *Handbook of photovoltaic science and engineering*, John Wiley & Sons **2010**.

[38] L. Z. Tan, F. Zheng, S. M. Young, F. Wang, S. Liu, A. M. Rappe, *npj Comput. Mater.* **2016**, *2*, 16026.

[39] P. R. Brown, D. Kim, R. R. Lunt, N. Zhao, M. G. Bawendi, J. C. Grossman, V. Bulovic, *ACS Nano* **2014**, *8*, 5863-5872.

[40] I. J. Kramer, L. Levina, R. Debnath, D. Zhitomirsky, E. H. Sargent, *Nano Lett.* **2011**, *11*, 3701-3706.

[41] C. M. Chuang, P. R. Brown, V. Bulović, M. G. Bawendi, *Nat. Mater.* **2014**, *13*(8), 796-801.

[42] X. Wang, J. Song, J. Liu, Z. L. Wang, *Science* **2007**, *316*, 102-105.

[43] J. I. Sohn, S. N. Cha, B. G. Song, S. Lee, S. M. Kim, J. Ku, H. J. Kim, Y. J. Park, B. L. Choi, Z. L. Wang, *Energy Environ. Sci.* **2013**, *6*, 97-104.

[44] S. Cha, S. M. Kim, H. Kim, J. Ku, J. I. Sohn, Y. J. Park, B. G. Song, M. H. Jung, E. K. Lee, B. L. Choi, J. J. Par, Z. L. Wang, J. M. Kim, K. Kim, *Nano Lett.* **2011**, *11*, 5142-5147.

[45] H. Yoon, H. Ryu, S. Kim, *Nano Energy* **2018**, *51*, 270-285.

[46] Y. J. Kim, J. Lee, S. Park, C. Park, C. Park, H. Choi, *RSC Adv.* **2017**, *7*, 49368-49373.

[47] S. Niu, X. Wang, F. Yi, Y. S. Zhou, Z. L. Wang, *Nat. Commun.* **2015**, *6*, 8975.

[48] H. Guo, M. Yeh, Y. Lai, Y. Zi, C. Wu, Z. Wen, C. Hu, Z. L. Wang, *ACS Nano* **2016**, *10*, 10580-10588.

[49] J. Lee, K. Y. Lee, M. K. Gupta, T. Y. Kim, D. Lee, J. Oh, C. Ryu, W. J. Yoo, C. Kang, S. Yoon, J. Yoo, S. Kim, *Adv. Mater.* **2014**, *26*, 765-769.

[50] M. Lu, J. Song, M. Lu, M. Chen, Y. Gao, L. Chen, Z. L. Wang, *Nano Lett.* **2009**, *9*, 1223-1227.

[51] K. Park, J. H. Son, G. Hwang, C. K. Jeong, J. Ryu, M. Koo, I. Choi, S. H. Lee, M. Byun, Z. L. Wang, K. J. Lee, *Adv. Mater.* **2014**, *26*(16), 2514-2520.

[52] Z. Lin, Y. Yang, J. M. Wu, Y. Liu, F. Zhang, Z. L. Wang, *J. Phys. Chem. Lett.* **2012**, *3*, 3599-3604.

[53] L. Persano, C. Dagdeviren, Y. Su, Y. Zhang, S. Girardo, D. Pisignano, Y. Huang, J. A. Rogers, *Nat. Commun.* **2013**, *4*, 1633.

[54] J. Lee, H. Yoon, T. Y. Kim, M. K. Gupta, J. H. Lee, W. Seung, H. Ryu, S. Kim, *Adv. Funct. Mater.* **2015**, *25*, 3203-3209.

[55] J. Wang, L. Pan, H. Guo, B. Zhang, R. Zhang, Z. Wu, C. Wu, L. Yang, R. Liao, Z. L. Wang, *Adv. Energy Mater.* **2018**, 1802892.

[56] K. Meng, J. Chen, X. Li, Y. Wu, W. Fan, Z. Zhou, Q. He, X. Wang, X. Fan, Y. Zhang, *Adv. Funct. Mater.* **2018**, 1806388.

[57] S. Qin, Q. Zhang, X. Yang, M. Liu, Q. Sun, Z. L. Wang, *Adv. Energy Mater.* **2018**, *8*, 1800069.

[58] Y. Cho, J. B. Park, J. Kim, J. Lee, W. Hong, I. Park, J. E. Jang, J. I. Sohn, S. Cha, J. M. Kim, *Nano Energy.* **2015**, *16*, 524-532.

[59] Y. Cho, D. Ahn, J. B. Park, S. Pak, S. Lee, B. O. Jun, J. Hong, S. Y. Lee, J. E. Jang, J. Hong, S. Y. Lee, J. E. Jang, J. Hong, S. M. Morris, J. I. Sohn, S. N. Cha, J. M. Kim, *Adv. Electron. Mater.* **2016**, *2*, 1600225.

[60] Y. Zi, J. Wang, S. Wang, S. Li, Z. Wen, H. Guo, Z. L. Wang, *Nat. Commun.* **2016**, *7*, 10987.

[61] B. Zhang, J. Chen, L. Jin, W. Deng, L. Zhang, H. Zhang, M. Zhu, W. Yang, Z. L. Wang, *ACS Nano* **2016**, *10*, 6241-6247.

[62] C. Xu, X. Wang, Z. L. Wang, *J. Am. Chem. Soc.* **2009**, *131*, 5866-5872.

[63] C. Pan, W. Guo, L. Dong, G. Zhu, Z. L. Wang, *Adv. Mater.* **2012**, *24*, 3356-3361.

[64] M. Lee, R. Yang, C. Li, Z. L. Wang, *J. Phys. Chem. Lett.* **2010**, *1*, 2929-2935.

[65] Y. Fang, J. Tong, Q. Zhong, Q. Chen, J. Zhou, Q. Luo, Y. Zhou, Z. Wang, B. Hua, *Nano Energy*, **2015**, *16*, 301-309.

[66] Y. Yang, H. Zhang, Y. Liu, Z. Lin, S. Lee, Z. Lin, C. P. Wong, Z. L. Wang, *ACS Nano*, **2013**, *7*, 2808-2813.

[67] Y. Yang, H. Zhang, Z. Lin, Y. Liu, J. Chen, Z. Lin, Y. S. Zhou, C. P. Wong, Z. L. Wang, *Energy Environ. Sci.* **2013**, *6*, 2429-2434.

[68] H. Guo, X. He, J. Zhong, Q. Zhong, Q. Leng, C. Hu, J. Chen, L. Tian, Y. Xi, J. Zhou, *J. Mater. Chem. A* **2014**, *2*, 2079-2087.

[69] G. W. Hwang, D. Kim, J. M. Cordero, M. W. Wilson, C. M. Chuang, J. C. Grossman, M. G. Bawendi, *Adv. Mater.* **2015**, *27*(30), 4481-4486.

[70] W. Wu, Z. L. Wang, *Nat. Rev. Mater.* **2016**, *1*, 16031.

[71] Z. L. Wang, W. Wu, C. Falconi, *MRS Bull.* **2018**, *43*, 922-927.

[72] W. Hu, C. Zhang, Z. L. Wang, *Nanotechnology.* **2018**, *30*, 042001.

[73] Y. Lin, W. Jian, *Nano Lett.* **2008**, *8*, 3146-3150.

[74] C. Lee, G. Lee, Van Der Zande, Arend M, W. Chen, Y. Li, M. Han, X. Cui, G. Arefe, C. Nuckolls, T. F. Heinz, J. Guo, J. Hone, P. Kim, *Nat. Nanotechnol.* **2014**, *9*, 676-681.

[75] T. Yajima, Y. Hikita, M. Minohara, C. Bell, J. A. Mundy, L. F. Kourkoutis, D. A. Muller, H. Kumigashira, M. Oshima, H. Y. Hwang, *Nat. Commun.* **2015**, *6*, 6759.

[76] B. W. Baugher, H. O. Churchill, Y. Yang, P. Jarillo-Herrero, *Nat. Nanotechnol.* **2014**, *9*, 262-267.

[77] J. S. Ross, P. Klement, A. M. Jones, N. J. Ghimire, J. Yan, D. Mandrus, T. Taniguchi, K. Watanabe, K. Kitamura, W. Yao, D. H. Cobden, X. Xu, *Nat. Nanotechnol.* **2014**, *9*, 268-272.

[78] F. Qian, Y. Li, S. Gradečak, H. Park, Y. Dong, Y. Ding, Z. L. Wang, C. M. Lieber, *Nat. Mater.* **2008**, *7*, 701-706.

[79] O. Lopez-Sanchez, D. Lembke, M. Kayci, A. Radenovic, A. Kis, *Nat. Nanotechnol.* **2013**, *8*, 497-501.

[80] S. N. Habisreutinger, L. Schmidt-Mende, J. K. Stolarczyk, *Angew. Chem. Int. Ed.* **2013**, *52*, 7372-7408.

[81] J. Luo, J. H. Im, M. T. Mayer, M. Schreier, M. K. Nazeeruddin, N. G. Park, S. D. Tilley, H. J. Fan, M. Gratzel, *Science.* **2014**, *345*, 1593-1596.

[82] Y. Hu, Y. Chang, P. Fei, R. L. Snyder, Z. L. Wang, *ACS Nano* **2010**, *4*, 1234-1240.

[83] Y. Hu, Y. Zhang, Y. Chang, R. L. Snyder, Z. L. Wang, *ACS Nano* **2010**, *4*(7), 4220-4224.

[84] Z. L. Wang, *Nano Today* **2010**, *5*, 540-552.

[85] C. Pan, L. Dong, G. Zhu, S. Niu, R. Yu, Q. Yang, Y. Liu, Z. L. Wang, , *Nature Photonics.* **2013**, *7*, 752-758.

[86] Y. Hu, Y. Zhang, L. Lin, Y. Ding, G. Zhu, Z. L. Wang, *Nano Lett.* **2012**, *12*, 3851-3856.

[87] Q. Yang, Y. Liu, C. Pan, J. Chen, X. Wen, Z. L. Wang, *Nano Lett.* **2013**, *13*, 607-613.

[88] Y. Yang, W. Guo, Y. Zhang, Y. Ding, X. Wang, Z. L. Wang, *Nano Lett.* **2011**, *11*, 4812-4817.

[89] Y. Liu, Q. Yang, Y. Zhang, Z. Yang, Z. L. Wang, *Adv. Mater.* **2012**, *24*, 1410-1417.

[90] J. Shi, P. Zhao, X. Wang, *Adv. Mater.* **2013**, *25*, 916-921.

[91] L. Dong, S. Niu, C. Pan, R. Yu, Y. Zhang, Z. L. Wang, *Adv. Mater.* **2012**, *24*, 5470-5475.

[92] Y. Zhang, Y. Yang, Z. L. Wang, *Energy Environ. Sci.* **2012**, *5*, 6850-6856.

[93] Y. Zhang, Z. L. Wang, *Adv. Mater.* **2012**, *24*, 4712-4718.

[94] M. Que, R. Zhou, X. Wang, Z. Yuan, G. Hu, C. Pan, *J. Phys. Condens. Matter* **2016**, *28*, 433001.

[95] L. Zhu, Z. L. Wang, *Adv. Funct. Mater.* **2018**, 1808214.

[96] D. Q. Zheng, Z. Zhao, R. Huang, J. Nie, L. Li, Y. Zhang, *Nano Energy* **2017**, *32*, 448-453.

[97] F. Boxberg, N. Søndergaard, H. Xu, *Nano Lett.* **2010**, *10*, 1108-1112.

[98] A. Golam Sarwar, R. Myers, *Appl. Phys. Lett.* **2012**, *101*, 143905.

[99] C. Pan, S. Niu, Y. Ding, L. Dong, R. Yu, Y. Liu, G. Zhu, Z. L. Wang, *Nano Lett.* **2012**, *12*, 3302-3307.

[100] S. Qiao, J. Liu, G. Fu, K. Ren, Z. Li, S. Wang, C. Pan, *Nano Energy.* **2018**, *49*, 508-514.

[101] L. Zhu, L. Wang, C. Pan, L. Chen, F. Xue, B. Chen, L. Yang, L. Su, Z. L. Wang, *ACS Nano.* **2017**, *11*, 1894-1900.

[102] C. Jiang, L. Jing, X. Huang, M. Liu, C. Du, T. Liu, X. Pu, W. Hu, Z. L. Wang, *ACS Nano.* **2017**, *11*, 9405-9412.

[103] L. Zhu, L. Wang, F. Xue, L. Chen, J. Fu, X. Feng, T. Li, Z. L. Wang, *Adv. Sci.* **2017**, *4*, 1600185.

[104] I. J. Kramer, G. Moreno-Bautista, J. C. Minor, D. Kopilovic, E. H. Sargent, *Appl. Phys. Lett.* **2014**, *105*, 163902.

[105] Y. Li, L. Wei, C. Wu, C. Liu, Y. Chen, H. Liu, J. Jiao, L. Mei, *J. Mater. Chem. A* **2014**, *2*, 15546-15552.

Yuljae Cho received his Bachelor degree in School of Electrical Engineering at Korea University in 2013 and DPhil degree in Department of Engineering Science at the University of Oxford in 2018. Currently, He is a postdoctoral researcher at the Department of Engineering Science at the University of Oxford. His research focuses on energy harvesting and optoelectronic devices based on inorganic quantum dots.

Sangyeon Pak received his Bachelor degree in Electrical Engineering at the University of Wisconsin – Madison in 2014 and DPhil degree in Department of Engineering Science at the University of Oxford in 2019. Currently, He is a postdoctoral researcher at the Institute of Basic Science and Department of Physics at Sungkyunkwan University. His research focuses on electronics and optoelectronics based on van der Waals structures.

Geon-Hyoung An is an assistant professor at the Department of Energy Engineering, Gyeongnam National University of Science and Technology, Korea. He received his Ph.D. from Material Science and Engineering from Seoul National University of Science and Technology. He was a postdoctoral researcher in the Department of Engineering Science at the University of Oxford. His research involves developing novel nanostructures for high-performance energy storage/conversion devices and investigating electrochemical behaviors of the electrode materials.

Bo Hou is a Senior Research Associate in the Department of Engineering at the University of Cambridge. He received his Ph.D. degree in the School of Chemistry at the University of Bristol (2010–2014) and worked as a postdoctoral researcher at the University of Oxford (2014-2018). His research interests include QD synthesis, QD optoelectronics, electron microscopy (TEM) and dynamic charge transfer analysis.

SeungNam Cha is an Associate Professor in the Department of Physics, Sungkyunkwan University. He received his Ph.D. in Electrical Engineering from the University of Cambridge and worked as a principal researcher at Samsung Advanced Institute of Technology (1996-2012) and an associate professor in Engineering Science at the University of Oxford (2014-2018). He has extensive research experience in the area of nanoelectronics, energy harvesting and display/lighting system.